

# Iridium optical constants from synchrotron reflectance measurements over 0.05- to 12-keV x-ray energies

D.E. Graessle<sup>\*a</sup>, R. Soufli<sup>b</sup>, A.J. Nelson<sup>b</sup>, C.L. Evans<sup>b</sup>, A.L. Aquila<sup>c</sup>, E.M. Gullikson<sup>c</sup>, R.L. Blake<sup>d</sup>,  
A.J. Burek<sup>e</sup>

<sup>a</sup>Smithsonian Astrophysical Observatory, MS-70, Cambridge, MA 02138-1516

<sup>b</sup>Lawrence Livermore National Laboratory, 7000 East Avenue, Livermore, CA 94550-9234

<sup>c</sup>Lawrence Berkeley Laboratory, 1 Cyclotron Rd, MS-2R0400, Berkeley, CA 94720

<sup>d</sup>RDS, PO Box 6880, Santa Fe, NM 87502-6880

<sup>e</sup>SFA Inc, Largo, MD 20774

## ABSTRACT

We present optical constants derived from synchrotron reflectance measurements of iridium-coated X-ray witness mirrors over 0.05-12 keV, relevant to the Chandra X-ray Observatory effective area calibration. In particular we present for the first time analysis of measurements taken at the Advanced Light Source Beamline 6.3.2 over 50-1000 eV, Chandra's lower-energy range. Refinements to the currently tabulated iridium optical constants (B. L. Henke et al., At. Data Nucl. Data Tables 54, 181-343, 1993 and on the Web at [http://www-cxro.lbl.gov/optical\\_constants/](http://www-cxro.lbl.gov/optical_constants/)) will become important as the low-energy calibration of Chandra's X-ray detectors and gratings are further improved, and as possible contaminants on the Chandra mirror assembly are considered in the refinement of the in-flight Ir absorption edge depths. The goal of this work has been to provide an improved tabulation of the Ir optical constants over the full range of Chandra using a self-consistent mirror model, including metallic layers, interface roughness, contaminating overlayer, and substrate. The low-energy data present us with a considerable challenge in the modeling of the overlayer composition, as the K-absorption features of C, O, and N are likely to be present in the ~10Å overlayer. The haphazard contamination and chemical shifts may significantly affect optical constants attributed to this overlayer, which will distort the iridium optical constants derived. Furthermore, the witness mirror contamination may be considerably different from that deposited on the flight optics. The more complex modeling required to deal with low-energy effects must reduce to the simpler model applied at the higher energies, which has successfully derived optical constants for iridium in the higher energy range, including the iridium M-edges, already used in the Chandra calibration. We present our current results, and the state of our modeling and analysis, and our approach to a self-consistent tabulation.

**Keywords:** iridium, optical constants, synchrotron radiation, reflectance, x-rays, Chandra X-ray Observatory

## 1 INTRODUCTION

When the Science Support Team for the Chandra X-ray Observatory (Chandra) selected iridium as the coating of choice for all four shells of the High Resolution Mirror Assembly (HRMA), they understood fully that their choice for superior reflecting efficiency in the 5-10 keV range would require a trade-off in the comfort and experience they had already gained using gold or nickel in previous missions. A portion of this trade was to be recovered by means of a separate coating calibration program, wherein a tunable, narrow-bandwidth source (e.g. synchrotron radiation) would be used to characterize the coatings in terms of their optical constants, using witness mirrors from the sixteen Chandra coating

---

\* [dgraessle@head.cfa.harvard.edu](mailto:dgraessle@head.cfa.harvard.edu); phone 1 617 495 7041; fax 1 617 495 7356; [hea-www.harvard.edu/~graessle](http://hea-www.harvard.edu/~graessle).

Copyright 2004 Society of Photo-Optical Instrumentation Engineers. This paper was published in *Optical Constants of Materials for UV to X-Ray Wavelengths*, Regina Soufli and John F. Seely, editors, Proceedings of SPIE vol. **5538**, p. 72, 2004, and is made available as an electronic reprint with permission of SPIE. One print or electronic copy may be made for personal use only. Systematic or multiple reproduction, distribution to multiple locations by electronic or other means, duplication of any material in this paper for a fee or for commercial purposes, or modification of the content of the paper are prohibited.

runs. What ensued was a major programmatic effort to characterize iridium optical constants thoroughly in the energy range of interest, 0.05-12 keV. The method used to derive the optical constants, and the consistency and quality of the results obtained, are the subject of this paper, intended to be the penultimate in a long series of progress reports on the results of this research.

The selection of DC-magnetron-sputtered iridium coatings for Chandra has born out well. The timely improved coating technologies for iridium, allowing thin layers to be deposited without excessive coating tension, while achieving nearly bulk material densities, have afforded the Chandra HRMA with two advantages. First, the coatings perform at or near the throughput levels predicted by the Chandra Calibration Team.<sup>1</sup> Second, the coatings are sufficiently uniform and dense to be characterized by optical constants without sacrificing certainty in the calibration to significant fitting errors. A third advantage is that the coatings are sufficiently pure and clean to allow a significant improvement in our knowledge of iridium optical constants over significant portions of the region of interest. Hence, in the energy range in question, this material is now as well understood as (or better than) any of its neighboring mirror materials in the Periodic Table, namely Au, Pt, Os, Re, or W. As proof of this point, we offer the following evidence.

### 1.1 Experimental details

The Chandra synchrotron calibration program has employed NSLS beamlines X8C (5000-12000 eV), X8A (2010-6200 eV), and U3A (940-2030 eV). For the 50-1300 eV range, with some overlap with U3A, we have used ALS Beamline 6.3.2. The beamlines<sup>2,3,4,5</sup> and reflectometers<sup>5,6</sup> have been described elsewhere. We shall restate here for reference that for the NSLS beamlines, double crystal monochromators were used. For the X8 beamlines, Si (111) crystals provided superb beam purity, throughput, and narrow energy bandwidth for the entire 2010-12000 eV range and beyond. For the U3A monochromator, rarely used Na  $\beta$ -alumina crystals performed extremely well, taking advantage of the high-energy cut-off of the NSLS VUV storage ring and the U3 upstream mirror to eliminate second-order contamination.

ALS Beamline 6.3.2, working in an energy region generally inaccessible to crystals at synchrotron intensities, employs a third-generation grating monochromator, with three variable line-spaced gratings, an order-sorter with a variety of mirror materials to minimize higher-order contamination, and thin film windows to eliminate stray light.

Also for future reference, the NSLS reflectometer worked in the *p*-polarization plane; the ALS 6.3.2 reflectometer works in the *s*-polarization plane. With respect to optical constants fitting, polarization becomes significant only in the lower energy range of ALS. For this paper, we have assumed 90% polarization in the relevant plane; we will investigate this issue further in future work on the ALS data in particular.

### 1.2 Reflectance measurements

The spectroscopy goals for the Chandra mission, which includes two medium-to-high resolution transmission gratings, require a calibration of the HRMA throughput that specifies all absorption features in detail. The goal of the calibration accuracy for the mission was to be within 1% at an arbitrary energy; this leaves less than 0.5% in the budget for synchrotron reflectance calibrations. The degree of detail required depends on the narrowness of the intrinsic features of the iridium, which were not known for most of the 0.05-12 keV range. Cosmic sources may have emission lines that are intrinsically vary narrow, depending on the source environments. However, the bandwidth of any double-crystal monochromator or grating monochromator is fixed once the geometry of the beam and crystal selection have been done. We claim that these parameters for the specific beamlines used were as near optimal as were available at the time.

Because the spectral detail was the driving factor in the calibration, we realized that reflectance-versus-energy scans would be the most essential data to be acquired. Nevertheless, to derive optical constants, which would allow a full calibration versus energy and angle in the modeling of the HRMA, detailed angle scans at fixed energy are the best method. However, the number of specific energies required, even for a single mirror, were far too great to allow the calibration to proceed with so many angle scans. For energy scans, the motion of the monochromator certainly adds some experimental noise to the measurements, due to vibration, wobble, and settling time. Taking detailed and relatively frequent direct scans of the monochromatic beam, with the mirror sample removed from the path, allow us to make reasonable estimates of these effects.

### 1.3 Modeling optical constants

The Chandra mirrors and witness mirrors are of Zerodur, coated with 325Å to 350Å of iridium on top of a 100Å chromium binding layer. These specifications necessitate a four-layer model (at least), including the substrate, binding underlayer, iridium layer, and a contaminating overlayer, as will occur with mirrors in common laboratory environments. While several different specifications of witness mirrors have been measured, we shall in this paper consider only one type, namely circular 2-inch disks of super-polished Zerodur, with less than one angstrom microroughness over 0.5-500  $\mu\text{m}$  spatial scales, and a flatness figure of  $\lambda/10$  ( $\lambda = 6328 \text{ \AA}$ ). These were produced by General Optical Co. of Moorpark, CA.

We have employed a fitting routine developed by D.L. Windt named *nkfit*, which is a precursor to the more elaborate and generally useful IMD software.<sup>7</sup> The tools run in IDL, and have been wrapped with a group of adaptive tools that allow rapid processing of energy scans at several angles for optical constant fitting at each energy. The several angle scans taken for alignment purposes are first fitted for not only optical constants of Ir, but also for layer depths and surface parameters (roughness). The procedure used for analysis of the angle scans has been described previously.<sup>8</sup> The roughness and interdiffusion have been successfully modeled only with the Nevot-Croce<sup>9</sup> interlayer model. Once these parameters have been determined from the particular angle scans relevant to that energy range, a fit for optical constants versus energy using the energy scans, with these layer and surface parameters fixed, is done. Only the Ir  $n (= 1-\delta)$  and  $k (= \beta)$  are free parameters in the fits of energy scan data.

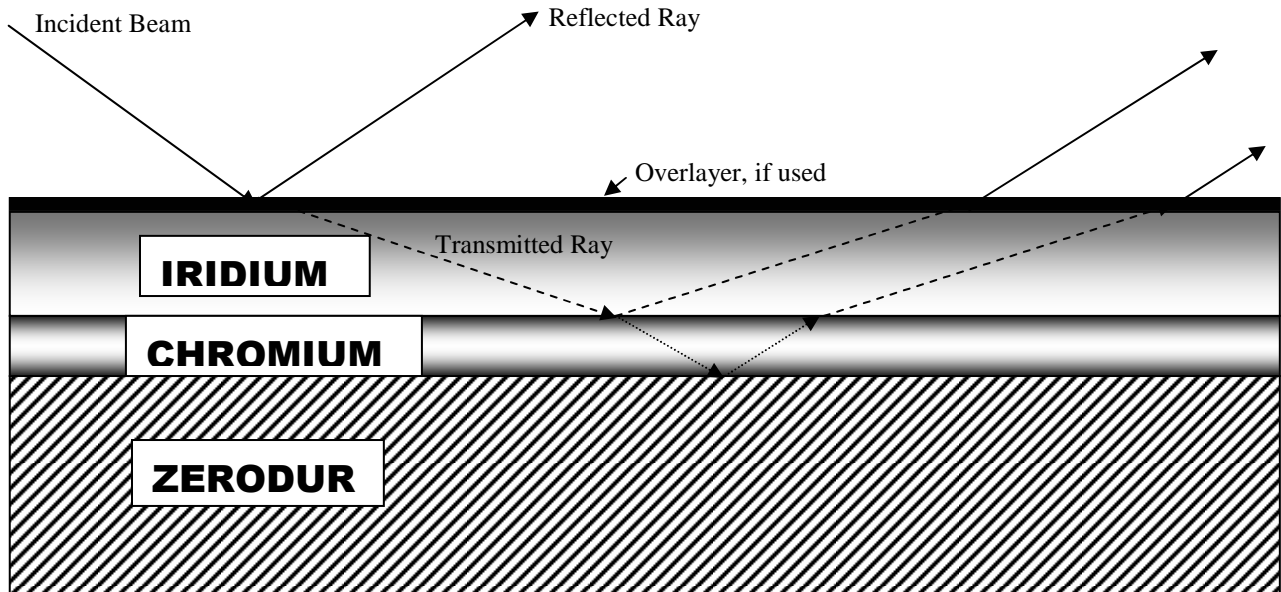


**Fig. 1:** The four-layer model incorporated into *nkfit* to derive optical constants for the Chandra witness mirrors.

## 2 DERIVED OPTICAL CONSTANTS FROM NSLS MEASUREMENTS

### 2.1 5-12 keV derived optical constants

The 5-12 keV energy range for this experiment was carried out at NSLS Beamline X8C. The data from X8C have been reported previously, and will be discussed only briefly.<sup>10</sup> The reflectance measurements obtained in this range for sixteen GO-type mirrors are extremely consistent, being within 0.5% excluding the interference fringes which are due to the Ir and Cr layer depths. Each of the 16 mirrors was coated in a separate coating run, and hence layer depths might reasonably be expected to vary within 10-15 angstroms run-to-run. The noise level for these measurements is within 0.25%. Hence one would still expect systematic variations between optical constants derived from each mirror

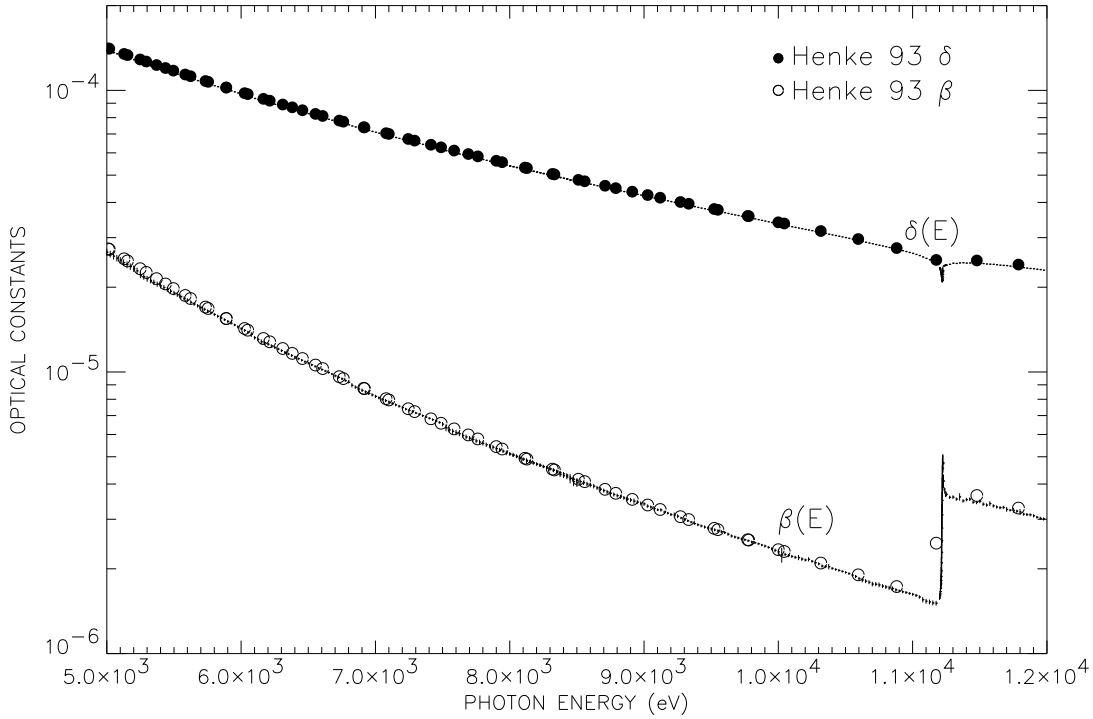


Fig. 2: Iridium optical constants derived from Beamline X8C (5-12 keV) for GO-type Chandra witness mirrors.

separately. The optical constants derived are shown in Fig. 2. Here the individual fitted results are plotted as vertical error bars, representing the standard deviation of the average of  $\delta(E)$  and  $\beta(E)$  derived from the 16 super-smooth mirrors. Tabulated values from the Henke-Gullikson tables<sup>11</sup> are given by the black dots and circle symbols in the figure. As the figure attests, our experimental results over 5-12 keV confirm the tabulated optical constants. The ~1.5% decrement of the experimental relative to the tabulated is likely an iridium coating density decrement of 1.5% below bulk on our witness mirrors. The bulk density of Ir is 22.39 g/cm<sup>3</sup>.

## 2.2 Optical constants over 2010-6200 eV

The previous section has dealt with a spectral region predominantly free of absorption features for iridium; the Ir L<sub>3</sub> edge (measured at 11.215 keV) is actually beyond the 0.07-10 keV region of interest for Chandra. The iridium absorption feature of primary concern for Chandra science capabilities is the M-edge region, which was covered in our experiment using NSLS Beamline X8A. The energy range of this beamline was subdivided into scan regions of 2010-2400 eV, 2250-2900 eV, 2800-4000 eV, and 3900-6200 eV, which provides adequate overlap between regions to check consistency. The troughs or minima of the iridium M-edges in reflectance were measured experimentally as follows: M<sub>5</sub>3d<sub>5/2</sub> at 2089 eV, M<sub>4</sub>3d<sub>3/2</sub> at 2156 eV, M<sub>3</sub>3p<sub>3/2</sub> at 2550 eV, M<sub>2</sub>3p<sub>1/2</sub> at 2909 eV, and M<sub>1</sub>3s at 3175 eV. The beamline energies for these points were confirmed by single crystal spectrometry to be accurate to one part in 10<sup>4</sup>.

Determination of the optical constants in this region requires inclusion of an overlayer in the model to optimize the fits of angle scans, and to reduce the mirror-to-mirror systematic variations in the resulting  $\delta(E)$  and  $\beta(E)$ . The overlayer introduces a masking effect, which tends to reduce the effect of the absorption in the optical constants. Because the overlayer deposition is quite random, the overlayer depths are not the same for each mirror, and hence some mirror-to-mirror scatter is introduced in these data. In Figs. 3 and 4, we present the optical constants derived from 16 mirrors over the 2010-5000 eV range as indicated, for cases including and not including an overlayer. The plotting method used is the same as for Fig. 2, wherein the experimental data points are vertical error bars representing the standard deviation of the average from the 16 mirrors at each energy. The tabulated optical constants from Ref. 11 are included as before. The overlayer for each mirror is derived from a fit to a 2550 eV reflectance-versus-angle scan. The overlayer material

assumed was a generic  $1\text{-g/cm}^3$  C-H<sub>2</sub> hydrocarbon chain with no other chemical elements included. The addition of the overlayer produces a slight decrease in the fitted value of  $\delta$ , but for  $\beta$  the effect is much more dramatic. Clearly the overlayer helps reduce the mirror-to-mirror systematic variations. It also reduces the systematic overlap errors seen at 2800-2900 eV and 3900-4000 eV markedly. The more detailed chemical composition of the overlayer is discussed in Sections 3 and 4.

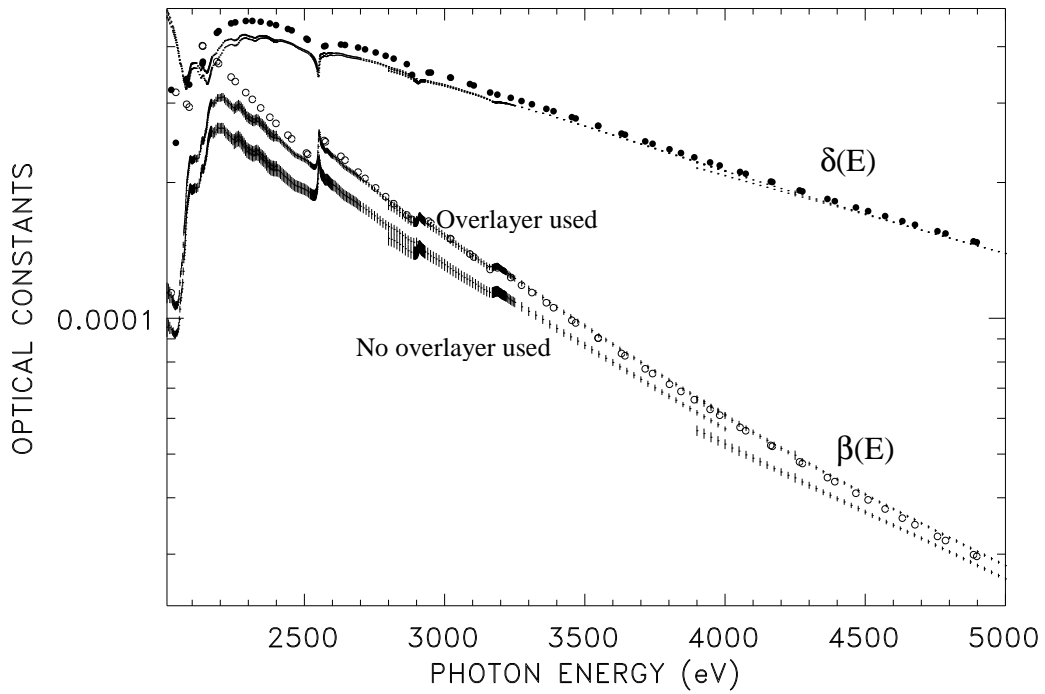


Fig. 3: Optical constants derived from reflectance measurements over 2010-5000 eV. Modeling with a C-H<sub>2</sub> overlayer not only improves fits, it also improves the overlaps at 3000 eV and 4000 eV. The symbols are Ref. 11 tabulated values.

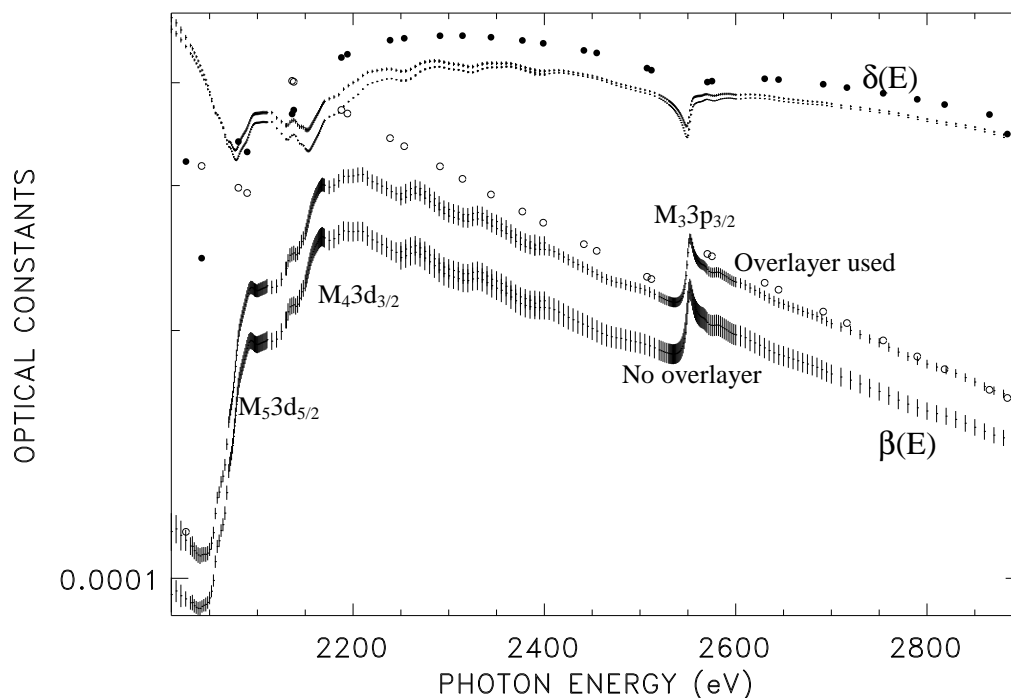


Fig. 4: Iridium optical constants derived from Beamline X8A (2010-2900 eV). For  $\delta(E)$ , the lower of the two traces near the top of the figure is the one derived using the overlayer. The symbols are Ref. 11 tabulated values.

The optical constants we have derived in the M-edge region show a considerably more complicated structure than is currently included in the atomic scattering tables for Ir. Not only are the  $M_5$  and  $M_4$  troughs displaced by some 40 eV from the tabulated binding energies, but there are additional extended features. We believe the apparent EXAFS on the  $M_4$  edge in particular is probably due to a bound-bound transition to an unoccupied outer shell electron level; hence this is an atomic effect. We shall clarify this in a future publication. In any case, Chandra gets the benefit of a more accurate representation of the absorption features from this work.

### 2.3 Optical constants over 940-2030 eV

The relatively low-absorption and featureless (for iridium) region leading up to the precursors for the Ir M-edges is considered next. Fig. 5 gives the optical constants results in a similar fashion as Figs. 3 and 4, wherein the results for modeling with and without an overlayer are included. Fig. 5 includes averages of only three mirrors, however. The U3A energy range was subdivided into two sub-ranges for this experiment, namely 940-1300 eV and 1280-2030 eV. The alignment and diagnostic angle scans for these sub-ranges were at 1200 eV and 1800 eV respectively. Hence the overlayer used was derived from analysis of angle scans at these energies, and applied to the energy scan data in the overlayer modeling case. The results with, versus without, an overlayer are similar to those in the previous section, namely that the effect for  $\delta(E)$  is not very significant, but  $\beta(E)$  is significantly influenced by the overlayer. In particular, the overlap error in  $\beta(E)$  at 1280-1300 eV is essentially eliminated when the overlayer is included in the model. However, the mirror-to-mirror variation is inconsistent going across this energy range, in some portions being smaller with the overlayer, and in other regions being greater. In either case, the spread is not very large, and the optical constants derived are experimentally well-determined. Nevertheless the results with overlayer match up very closely with the tabulated values in this region of relatively low Ir absorption. The case having been made, we shall consider only analysis using the overlayer for the remainder of this paper.

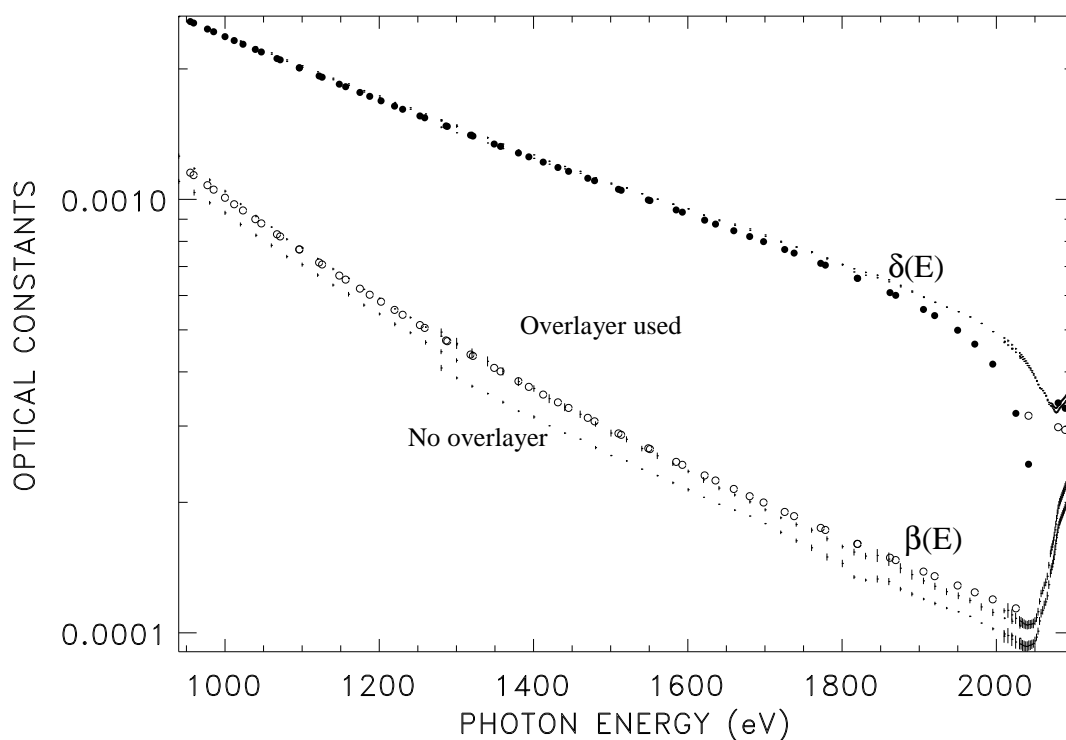


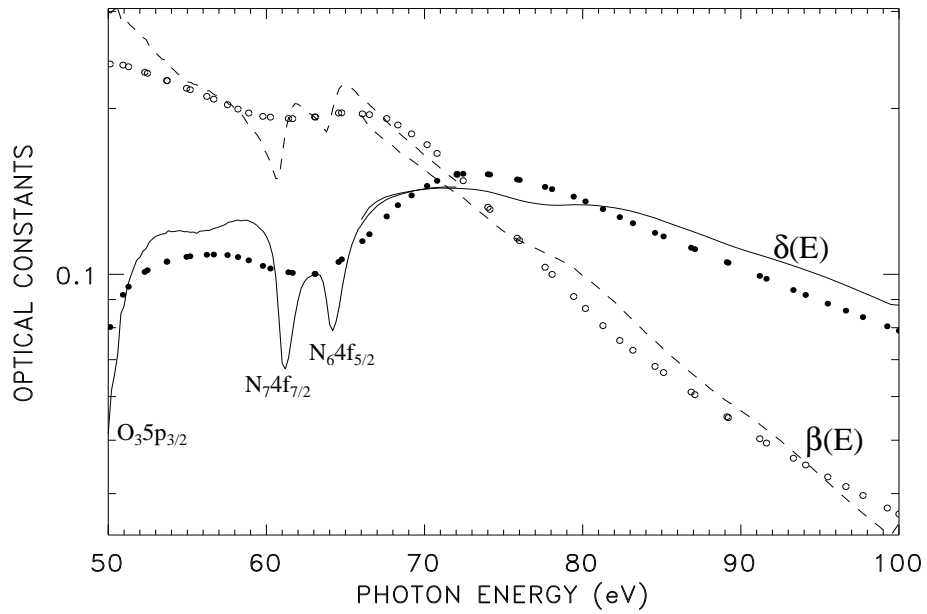
Figure 5: Iridium optical constants derived from U3A reflectance data (940-2030 eV). Note the good overlap obtained with the X8A data over 2010-2030 eV. Overlap at 1280-1300 eV is improved again with an overlayer in the model. The symbols are Ref. 11 tabulated values.

### 3 DERIVED OPTICAL CONSTANTS FROM ALS 6.3.2

Only two of our super-smooth witness mirrors were measured on ALS Beamline 6.3.2, and only one of them for the full energy range. Figures 6 through 9 give the optical constants results, with an overlayer included in the model, for one or both mirrors, with tabulated constants indicated as well. The overlayer used was that derived from angle scans at 1300 eV from Beamline U3A, as in the previous section. Particularly in Figs. 6 and 7, there are strong indications that our work will provide a significant enhancement in the detailing of optical constants for iridium, in that iridium N- and O-absorption edges and extended absorption features are visible. However, for the 50-283 eV range, which is below the carbon K-edge, we may be relatively free of strong contaminant absorption. Hence the deviations from tabulated such as are seen over 100-200 eV (Fig. 7) are likely indicators of improved optical constants for Ir. We note however, that the apparently pointed feature in the energy overlap at 141-147 eV is spurious.

Insasmuch as this is a work in progress, these results are still preliminary and further work is needed to deconvolve the effects of the overlayer. Recall that in our model, the overlayer material assumed includes only C-H<sub>2</sub>. Most of the serious contaminant absorption effects will be visible in Fig. 8, which covers the carbon, nitrogen, and oxygen K-edges. The effects due to carbon absorption are obvious at 284 eV, even with the overlayer included. Hence it may be that the overlayers applied to these two mirrors is inadequate. The oxygen K-edge effects begin to be seen at about 535 eV experimentally. The beamline transmission is also strongly influenced by absorption, which can make beam spectral purity and input flux normalization problematic, as is common with beamlines in this range. We shall endeavor in our future work to disentangle as much information as possible at these C and O edges, but we may in the end need to

interpolate our results through these short regions. Clearly we require additional information about the composition of the overlayer. (See Section 4.)



Figs: 6: Optical constants from a single witness mirror compared with tabulated, in the region of the O, N7, and N6 edges, plus the extended feature at 77-79 eV. The overlap error in  $\beta(E)$  is large over 66-72 eV. The symbols are Ref. 11 tabulated values.

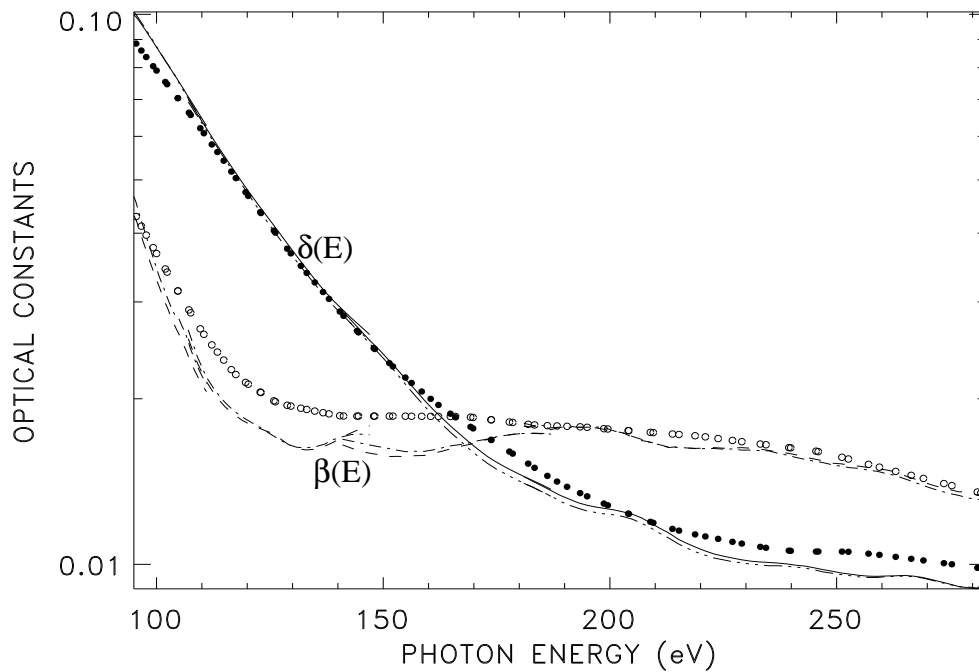


Fig. 7: Optical constants from two mirrors in a region dominated by Ir N- and O- edge extended absorption. The feature at the overlap at 141-147 eV is probably spurious. However the systematic displacement from tabulated is probably a real measurement for Ir. The symbols are Ref. 11 tabulated values.

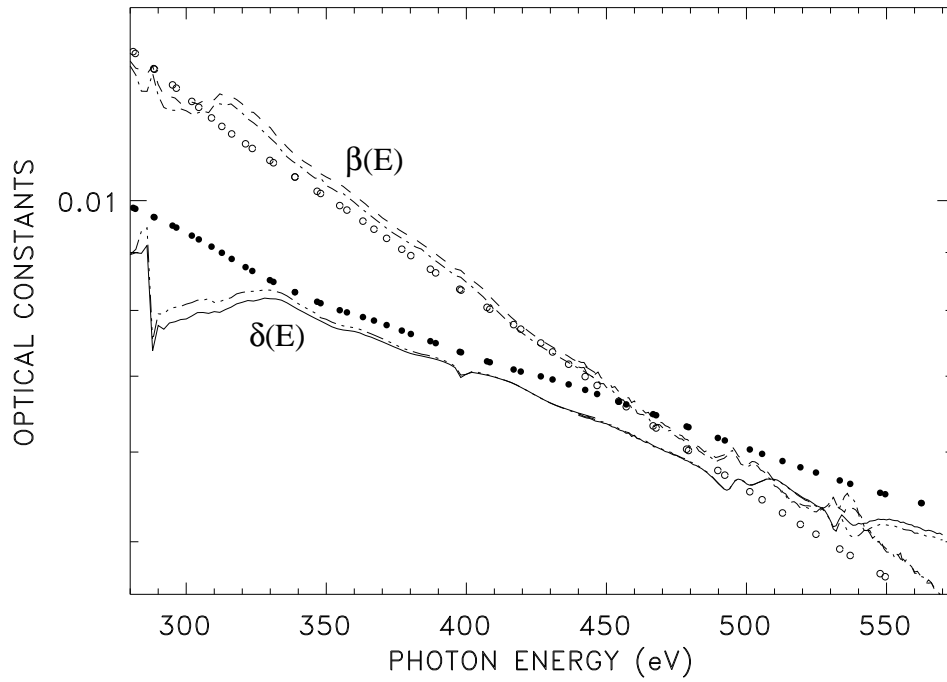


Fig. 8: Optical constants from two mirrors in a region where obvious contaminating elements are present, and likely to be in the overlayer. The symbols are Ref. 11 tabulated values.

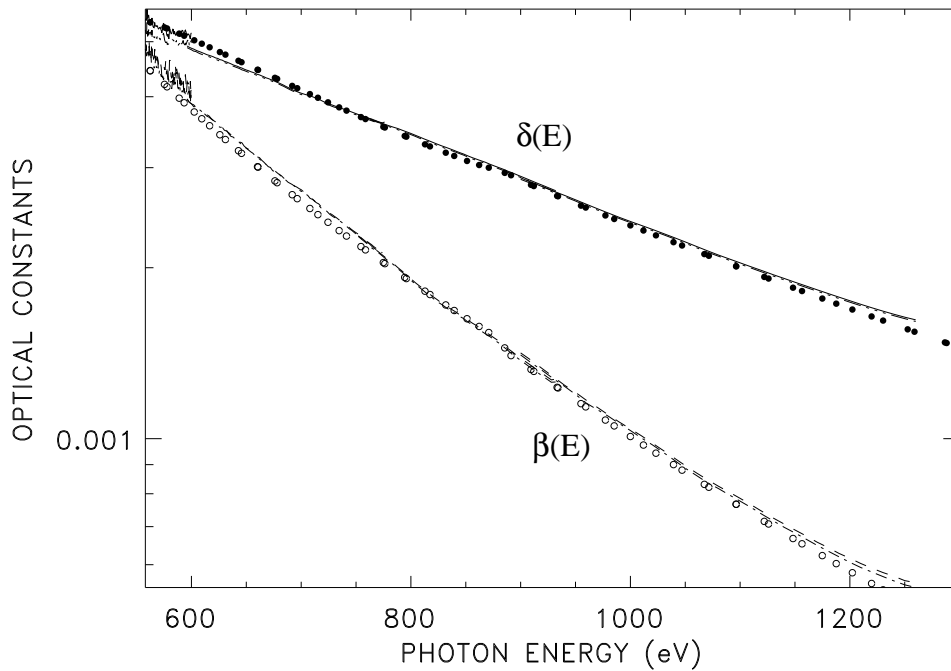


Fig. 9: Optical constants derived from two mirrors in the featureless region at the upper end of the 6.3.2 accessible energy range. The results are not as clean and well-defined as in the case of Fig. 2, but overlayer chemistry is not likely to be much of a factor here.

We do not want to overlook the Iridium  $N_{3/2}$  edge which appears at 495 eV and includes a double modulation in the traces at that point. Also, at 395 eV there is a clear but unidentified feature in the  $\delta(E)$ , which is near but not precisely at the expected position for N-K. The feature appears to be a contaminant unaccounted for in the model; it is unlikely to be associated with iridium. The final portion of the ALS 6.3.2 energy range is presented in Fig. 9, where no striking features occur, and the experimental values do not greatly deviate from the tabulated.

#### 4 XPS MEASUREMENTS

Especially in the extreme ultraviolet wavelength region, the reflectance method is sensitive to even thin layers (a few Å) of surface contamination. In the previous Section it is explained how it is necessary to assume a generic hydrocarbon overlayer for each mirror surface, in order to adequately fit the optical constants delta, beta from reflectance measurements. It is not surprising that such overlayers should form on the Chandra witness mirror samples, given their frequent handling in air and their being subject to repeated pump down and venting processes during reflectance measurements at various synchrotron facilities, as is discussed in Section 1.1. Nevertheless, until recently the Chandra witness mirrors had never been evaluated quantitatively for surface contamination effects (native oxide, hydrocarbons) using an independent method. For this purpose, surface analysis was performed by means of X-ray Photoemission Spectroscopy (XPS) on two of the iridium witness mirrors (2-inch diameter Zerodur substrates polished by General Optics). These are the same two mirrors whose optical constants are presented in Figs. 7-9. XPS was performed using a "Physical Electronics Quantum 2000 Scanning ESCA Microprobe" system at Lawrence Livermore National Laboratory. Briefly, this method consists of illuminating an area on the sample (in this case (in this case a spot with 100  $\mu\text{m}$  diameter) with monoenergetic x-rays (in this case  $h\nu = 1486.7$  eV, Al  $K_{\alpha}$  source) and by analyzing the emitted photoelectrons with an electron spectrometer according to their kinetic energy  $E_k$ . The presence of an element on the sample surface is identified by the binding energy  $E_b = h\nu - E_k$  of its atomic core electrons. The analyzer is normally operated as an energy "window", accepting only those electrons having an energy within this fixed window, referred to as "pass energy". Investigating different energies is accomplished by applying a variable electromagnetic field on the photoelectrons before they reach the analyzer. An inspection of the spectrum after an energy scan provides information on the elemental composition and chemical state of the sample surface. The results are shown in the form of peak areas, as a function of electron binding energy  $E_b$ . Each area under a peak, which represents the integrated photoelectron signal, is proportional to the concentration of a specific element in the surface region of the sample. Two types of scans were used in this experiment: (i) Fast, low resolution ("survey") scans, with a pass energy of 187.85 eV, and (ii) slower, high-resolution ("multiplex") scans, with a pass energy of 23.5 eV for a more detailed study of the peaks.

Figure 10 shows the XPS survey scan results from one of the two mirrors: in addition to the iridium-related peaks that are expected due to the iridium coating, there is evidence of oxygen, nitrogen, carbon and silicon (from the O 1s, N 1s, C 1s and Si 2s peaks respectively) on the mirror surface. Nitrogen and silicon appear to be present in trace amounts only. Nitrogen was the gas used to vent the vacuum reflectometers at both ALS and NSLS synchrotron facilities where this mirror was measured. The presence of silicon could be attributed to a silicate grease that was used in the NSLS reflectometer while this mirror was being measured. A more detailed inspection of the carbon and oxygen peaks is shown in the spectra of the XPS multiplex scans in Figure 11. Results from both mirrors are shown for each element, demonstrating that the level of oxygen and carbon contamination is rather consistent between the two mirrors. The XPS spectra in Figure 11 (top curves) were used to calculate the surface coverage of oxygen and carbon atoms for one of the mirrors, using the expression<sup>12</sup>:

$$\frac{Y_o}{Y_s} = \frac{\mu_o M_s \sigma T}{\mu_s \rho_s N L \cos \phi} \quad (1)$$

where  $Y_o$ ,  $Y_s$  are the integrated photoelectron signals from the overlayer (O 1s or C 1s peak) and substrate (Ir 4d peak) respectively, obtained as results of a multiplex scan;  $\mu_o$ ,  $\mu_s$  (barns/atom) are the overlayer and substrate photoionization cross sections respectively;  $\sigma$  (atoms/cm<sup>2</sup>) is the surface coverage of overlayer atoms;  $M_s$  (g/mol),  $\rho_s$  (g/cm<sup>3</sup>) are the molecular weight and the mass density of the substrate material (iridium), respectively;  $L$  is the escape depth for the substrate (Ir 4d) photoelectrons;  $\phi$  is the angle of photoelectron collection by the analyzer with respect to the sample normal ( $\phi = 45^\circ$  in this case);  $N$  is Avogadro's number ( $N = 6.022 \times 10^{23}$  molecules/mol). The factor  $T$  accounts for the transmission efficiency of the analyzer, which in operation mode of constant pass energy, is given by

$$T = \frac{h\nu - E_{b,s}}{h\nu - E_{b,o}} \quad (2)$$

where  $E_{b,o}$ ,  $E_{b,s}$  are the binding energies of overlayer and substrate materials respectively. For the iridium substrate,  $M_s = 192.22$  g/mol,  $\rho_s = 22.4$  g/cm<sup>3</sup>. From the XPS multiplex scans at  $h\nu=1486.7$  eV, for the Ir 4d substrate peak:  $E_{b,s} = 295.35$  eV,  $Y_s = 97816$  counts $\times$ eV/sec,  $\mu_s = 0.2542$  barns/atom; for the O 1s overlayer peak:  $E_{b,o} = 530.46$  eV,  $Y_o = 12397$  counts $\times$ eV/sec,  $\mu_o = 0.040$  barns/atom; and for the C 1s overlayer peak:  $E_{b,o} = 283.4$  eV,  $Y_o = 6056$  counts $\times$ eV/sec,  $\mu_o = 0.013$  barns/atom. Finally, it is estimated that the escape depth for the Ir 4d photoelectrons should be  $L \approx 15$  Å, with an error bar of at least  $\pm 20\%$ .<sup>13</sup> After substituting equation (2) in equation (1) and solving for the overlayer surface coverage  $\sigma$  using the values presented above, the result for oxygen is  $\sigma = 4.8 \times 10^{15}$  atoms/cm<sup>2</sup> and for carbon  $\sigma = 9.1 \times 10^{15}$  atoms/cm<sup>2</sup>, revealing a 1:2 ratio between oxygen and carbon atomic coverage on the mirror surface. Further analysis and fitting of the peaks obtained from the XPS multiplex scans shows that the O 1s peak pertains to two bonding states, C-O and Ir-O. Similarly, the C 1s peak shape indicates the presence of C-H and C-O. These results demonstrate the presence of a hydrocarbon-type overlayer in addition to some oxidation on the mirror surface, and justify the need for use of such overlayer in the fitting of experimental reflectance data in the previous Section. The XPS analysis results presented in this Section became available shortly before the present manuscript was due for publication. Thus we did not have the chance to implement them to obtain a quantitative estimate of the thickness and composition of the overlayer used in the fitting of the optical constants of iridium presented herein. We hope to be able to complete this task in a future publication.

## 5 SUMMARY

We have presented our current results for iridium optical constants for the full calibration range of Chandra, specifically 0.05-12 keV x-ray energies. The results for the 0.7-12 keV range are in all likelihood final or very nearly final, pending further evaluation of the overlayer XPS measurements, and we have made significant contributions to improve the optical constants in the M-edge region for iridium in particular. Below 700 eV, there is still work to be done to deconvolve the effects of what is now a reasonably well-determined overlayer in terms of its composition. We shall be working toward a self-consistent model for that overlayer on a mirror-by-mirror basis, in an attempt to determine whether a consistent depth can be used, or if variations in the layer depth at the several angle scan energies may be accounted for by its inherent spatial nonuniformity. In any case, we state here for the record that the Chandra synchrotron witness mirror calibration program has been fully successful, and that a formal journal publication is forthcoming to report our final results.

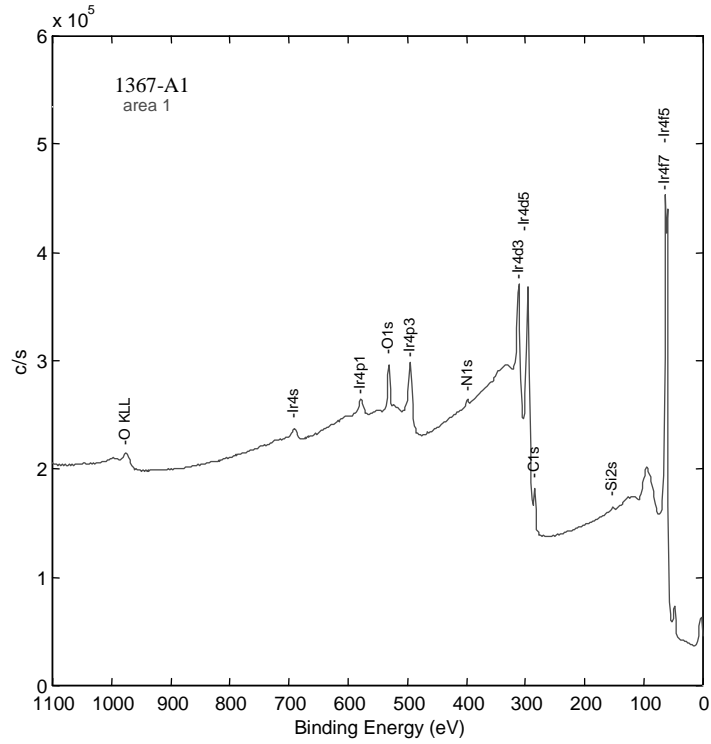


Figure 10: Survey XPS scan obtained from one of the Chandra witness mirrors.

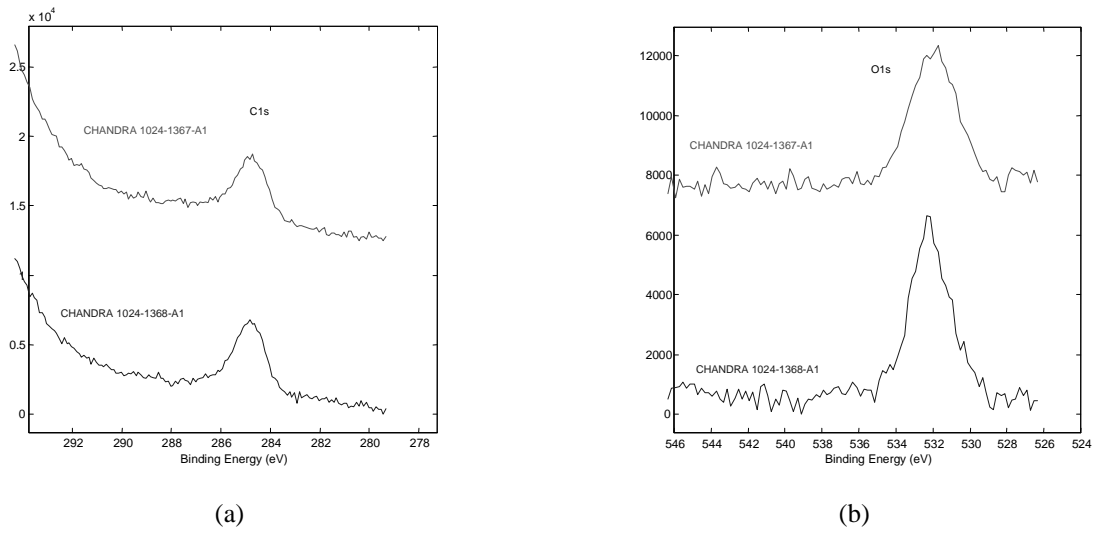


Figure 11: High-resolution, “multiplex” XPS spectra for the C 1s (a) and O 1s (b) peaks. Results from two Chandra witness mirrors are shown in each plot. The analysis and calculations presented in this manuscript refer to XPS results from the 1024-1367-A1 mirror (top curves).

## ACKNOWLEDGEMENTS

The following individuals have participated in laboratory engineering, planning, measurements, or analysis for Chandra synchrotron reflectance calibrations, over the ten-year period of the planning and execution of this task, and we hereby express our gratitude for their participation: T. H. Burbine, G. Chartas, A.M. Clark, J.P. Cobuzzi, J.J. Fitch, R. Francoeur, B. Harris, R.H. Ingram, J.Z. Juda, A.G. Roy, D.A. Schwartz, E.S. Sullivan, J.B. Sweeney, and P. Zhao. Beamline scientists and technicians such as M. Sagurton (X8A), R. Alkire (X8C), S. Mrowka and Andreas Stonas (ALS 6.3.2) also contributed advice and assistance when needed. This list is not exhaustive, but includes the main participants. The authors are grateful for discussions and encouragement provided by the late L.P. Van Speybroeck, whom we remember fondly.

This work is supported by NASA (Contract Nos. NAS8-40224 and NAS8-39073) and by the US D.O.E. The Department of Energy supports the National Synchrotron Light Source (NSLS) at Brookhaven National Laboratory, and the Advanced Light Source (ALS) at Lawrence Berkeley Laboratory. This work was performed under the auspices of the U.S. Department of Energy by the University of California Lawrence Livermore National Laboratory under Contract No. W-7405-ENG-48. The work performed at Lawrence Berkeley National Laboratory was supported by the U.S. Department of Energy under contract No. DE-AC03-76F00098.

## REFERENCES

1. P. Zhao, D. Jerius, R.J. Edgar, T.J. Gaetz, L.P. Van Speybroeck, B. Biller, E. Beckerman, and H.L. Marshall, "Chandra X-ray Observatory mirror effective area," in *Proc. SPIE*, **5165**, pp. 482-496, 2003.
2. NSLS Beamline X8A web page <http://www.bnl.gov/u3cx8a/X8A.htm>.
3. A.J. Burek, R.L. Blake, J.P. Cobuzzi, J.J. Fitch, R. Francoeur, D.E. Graessle, R.H. Ingram, E.S. Sullivan, and J.B. Sweeney, "The development of Beamline U3A for AXAF synchrotron reflectivity calibrations," in *X-ray Optics, Instruments, and Missions*, ed. R.B. Hoover and A.B.C. Walker II, *Proc. SPIE*, **3444**, pp. 584-597, 1998.
4. W.J. Trela, R.J. Barlett, F.D. Michaud, and R. Alkire, "An X-ray Beamline for the energy range 5-20 keV," *Nucl. Inst. and Meth.* **A266**, pp. 234-237, 1988.
5. J.H. Underwood, E.M. Gullikson, M. Koike, and P.J. Batson, "Beamline for metrology of X-ray/EUV optics at the Advanced Light Source," *Proc. SPIE*, **3113**, pp. 214-221, 1997.
6. D.E. Graessle, J.J. Fitch, R.H. Ingram, J.Z. Juda, and R.L. Blake, "A reflectometer end station for synchrotron calibrations of AXAF flight optics and for spectrometric research applications," *Proceedings of the 5<sup>th</sup> International Conference on Synchrotron Radiation Instrumentation*, ed. J.B. Hastings, S.L. Hulbert, and G.P. Williams, Stony Brook, NY, July 1994, *Rev. Sci. Instr.* **66**(2) Part II, pp. 18-31, 1996.
7. D.L. Windt, "IMD-software for modeling the optical properties of multilayer films," *Computers Phys.* **12**, 360-370, 1998. The IMD program is available at <http://www.cletus.phys.columbia.edu/~windt/imd/>.
8. D.E. Graessle, R. Soufli, A.L. Aquila, E.M. Gullikson, R.L. Blake, A.J. Burek, "Iridium optical constants for the Chandra X-ray Observatory from reflectance measurements of 0.05-12 keV," in *Proc. SPIE*, **5165**, pp. 469-481, 2003.
9. L. Nevot and P. Croce, "Caracterisation des surfaces par reflexion rasante de rayons X. Application a l'etude du polissage de quelques verres silicates," *Rev. Phys. Appl.* **15**, pp. 761-779, 1980.
10. D.E. Graessle, R.L. Blake, A.J. Burek, S.E. Dyson, J.J. Fitch, D.A. Schwartz, and R. Soufli, "Modeling of synchrotron reflectance calibrations of AXAF iridium-coated witness mirrors over 2-12 keV," in *X-ray Optics, Instruments, and Missions*, ed. By R.B. Hoover and A.B.C. Walker II, *Proc. SPIE*, **3444**, pp. 140-159, 1998.
11. B.L. Henke, E.M. Gullikson, and J.C. Davis, "X-ray interactions: photoabsorption, scattering, transmission, and reflection at E=50-30,000 eV, Z=1-92," in *Atomic Data and Nuclear Data Tables* **54**(2), p. 181, 1993. See also the Web page [http://www-cxro.lbl.gov/optical\\_constants/](http://www-cxro.lbl.gov/optical_constants/).
12. A.F. Carley and M.W. Roberts, "An X-ray photoelectron spectroscopic study of the interaction of oxygen and nitric oxide with aluminum", *Proc. R. Soc. London Ser. A* **363**, 403-424 (1978).
13. M. P. Seah and W. A. Dench, "A Standard Data Base for Electron Inelastic Mean Free Paths in Solids", *Surface and Interface Analysis*, **1**, 2-11 (1979).